Fully depleted emitter layers: a novel method to improve band alignment in thin-film solar cells

BG Mendis[1]

1. Dept. of Physics, Durham University, South Road, Durham, DH1 3LE, UK

Abstract

The interface between the emitter and absorber layers in a thin-film solar cell must satisfy two important criteria, namely a small lattice mismatch and electron barrier height. It is shown that the barrier height is lowered when the emitter is fully depleted of free electron carriers by making the layer thinner than its space charge region, thereby enhancing thermionic emission of the photocurrent across the interface. Lattice matching is therefore the only requirement for a fully depleted emitter. The concept is applied to a lattice matched ZnS-Cu_2ZnSnS_4 (CZTS) interface which has a large intrinsic barrier height. Recent experimental evidence however suggest that ZnS becomes current unblocking when sufficiently thin. The theoretical efficiency for fully depleted ZnS is as high as 16.1%, due to the combination of a large open circuit voltage (1.0 V) from lattice matching and reasonable short circuit current density (24 mA/cm^2). Lattice matched GaP and AlP are also potential CZTS emitter layers in the fully depleted configuration. The possibilities for exploring new materials combinations are therefore greater with fully depleted emitters. Furthermore, the concept can in principle be applied to any thin-film solar cell, making it highly versatile.

1. Introduction

Materials selection for device applications typically require optimising several parameters simultaneously, which is difficult to achieve in practice. An example of this is the heterojunction interface between the *p*-type absorber and *n*-type emitter layer in a thin-film solar cell (Figure 1a). Light is absorbed within the absorber layer to generate electron-hole pairs. Electrons that reach the space charge region are extracted via the built-in electric field at the absorber-emitter heterojunction. If there is lattice mismatch at the heterojunction (Figure 1b) the defect states within the band gap can act as local recombination sites, thereby reducing the extracted photocurrent (e.g. CdS-CdTe thin-film solar cells [1]). On the other hand the heterojunction may be lattice matched, but has a large conduction band (CB) offset, which acts as an energy barrier impeding current flow (Figure 1c). Examples for this kind of system includes ZnS-Cu_2ZnSnS_4 (CZTS) [2-3]. In fact many current thin-film solar cell devices have non-ideal interfaces, where the lattice mismatch and/or CB offset is not optimised. Even a partial relaxation of the stringent materials demands is desirable, so that new materials combinations can be explored that ultimately lead to higher efficiency.

Here fully depleted emitter layers are proposed as a method to relax the requirement of a small CB offset. The absorber and emitter layers should therefore only be lattice matched in order to create a fit for purpose heterojunction. The emitter layer is made thinner than its internal space

charge region, so that the entire layer is depleted of free electrons. The modified electric field within the absorber layer reduces the barrier due to any intrinsic CB offset, so that *thermionic emission* of the photocurrent becomes possible. The concept is quite general, but here it is demonstrated on a ZnS-CZTS heterostructure. CZTS is based on earth abundant, non-toxic elements and is therefore an ideal candidate for future Tera Watt scale electricity generation [4]. The highest cell efficiency has however plateaued at 12.6% [5], significantly below other thin-film technologies, such as CdTe and $Cu(In,Ga)Se_2$. Novel strategies for improving CZTS efficiency are therefore urgently required. The CdS emitter-CZTS interface in current devices is a strong contributing factor to the low efficiency [6,7], as evidenced by a low activation energy extracted from open circuit voltage (V_{oc}) vs. temperature measurements [6,8]. The *pn*-heterojunction can be optimised by replacing CdS with thin, fully depleted ZnS, thereby overcoming the current blocking effect that is otherwise present in bulk ZnS due to the intrinsic CB offset [2-3]. The phenomenon of current unblocking in thin ZnS layers is consistent with several recent experimental studies [9-11]. Furthermore, the lattice coherency at the ZnS-CZTS interface is expected to increase the V_{oc}, which is otherwise extremely poor for even the highest efficiency CZTS devices [6]. Parasitic series and shunt resistances can be an issue with ultra-thin emitter layers and in such cases ZnS can be used as a buffer layer, sandwiched between CdS and CZTS, to produce a similar result (see below).

2. Theory of fully depleted emitter layers

In this section the theory of fully depleted emitter layers is described using the ZnS-CZTS model system. Figure 2a shows the band edge diagram for *p*-type CZTS and *n*-type ZnS (the latter can be produced via Al-doping [12]), before making contact. Note the large (1.3 eV; [3]) CB offset between CZTS and ZnS which is responsible for the electron blocking behaviour discussed previously. The band edge diagram after the two semiconductors have made contact is shown in Figure 2b. The barrier height $\phi_B = \Delta E_F + \Delta\chi - e\Delta V_{CZTS}$, where ΔE_F is the energy difference between the Fermi level and CB minimum in the CZTS quasi-neutral region, $\Delta\chi$ is the difference in electron affinity between absorber and emitter layers, e is the electron charge and ΔV_{CZTS} is the potential change due to band bending within CZTS. A larger value for ΔV_{CZTS} therefore reduces the barrier for electron transport via thermionic emission. The space charge width (x_n) within ZnS is between 0.4-4.5 μm for doping concentrations in the range 10^{14}-10^{16} cm^{-3} and is larger than the ZnS precipitates typically observed in CZTS [2, 13-14]. A more realistic calculation should therefore consider a fully depleted ZnS layer.

Two criteria must be satisfied when different semiconductors are brought into contact and achieve equilibrium. The first is a constant Fermi level so that there is no net current. This is achieved through charge redistribution, while maintaining charge neutrality (second criterion). When ZnS is fully depleted however there are not enough ionised donors to simultaneously maintain a constant Fermi level and charge neutrality. A potential solution is that excess charge could build up in defect regions, such as free surfaces and interfaces. In effect the equilibrium Fermi level would not be aligned with the quasi-neutral level for the defect, causing the defects to acquire net charge. In fact this is the origin of charged grain boundaries in semiconductor materials [15], and a similar mechanism should also be valid for free surfaces and interfaces.

The CZTS-ZnS heterointerface is however coherent [16], so that there are no significant energy levels within the band gap. Therefore the excess positive charge σ must build up at the ZnS 'free surface', as indicated in Figure 2c for a fully depleted ZnS layer of thickness d. This surface charge is also essential for maintaining zero electric field outside the device (see below).

The heterojunction properties are calculated using Poisson's equation:

$$-\frac{d^2V}{dx^2} = \frac{dE}{dx} = \frac{\rho(x)}{\varepsilon} \qquad \ldots (1)$$

where V, E and ρ are the potential, electric field and charge density respectively, ε is the dielectric constant and x is the position coordinate ($x = 0$ is at the heterojunction, while CZTS is on the $x > 0$ side). Within the ZnS region in Figure 2c:

$$\rho(x) = N_d e + \sigma e \delta(x + d) \qquad \ldots (2)$$

where σ is the surface charge density at $x = -d$, N_d is the ZnS donor concentration and δ is the Dirac delta function. The electric field within ZnS follows from Eqs. (1) and (2):

$$E_{\mathrm{ZnS}}(x) = \frac{N_d e(x + d)}{\varepsilon_{\mathrm{ZnS}}} + \frac{\sigma e}{\varepsilon_{\mathrm{ZnS}}} \qquad \ldots (3)$$

E_{ZnS} was derived taking into account the boundary condition at $x = -d$, namely that $D_{\mathrm{ZnS}}(x = -d) = \sigma e$, where $D(x) = \varepsilon E(x)$ is the electric displacement (note that the electric field at $x < -d$ is zero). The first term in Eq. (3) represents the electric field due to ionised donors, while the second term is due to the surface charge. The electric field within CZTS can similarly be shown to be:

$$E_{\mathrm{CZTS}}(x) = \frac{N_a e}{\varepsilon_{\mathrm{CZTS}}}(x_p - x) \qquad \ldots (4)$$

where x_p is the CZTS space charge width and N_a is the CZTS acceptor concentration. Applying the boundary condition $D_{\mathrm{ZnS}}(0) = D_{\mathrm{CZTS}}(0)$ at the heterojunction at $x = 0$ gives:

$$N_d d + \sigma = N_a x_p \qquad \ldots (5)$$

This indicates that charge is conserved. The potential change within ZnS (ΔV_{ZnS}) is obtained from Eqs. (1) and (3):

$$\Delta V_{\mathrm{ZnS}} = \frac{N_d e d^2}{2\varepsilon_{\mathrm{ZnS}}} + \frac{\sigma e d}{\varepsilon_{\mathrm{ZnS}}} \quad \ldots (6)$$

and similarly for ΔV_{CZTS}:

$$\Delta V_{\mathrm{CZTS}} = \frac{N_a e x_p^2}{2\varepsilon_{\mathrm{CZTS}}} \quad \ldots (7)$$

The sum of ΔV_{ZnS} and ΔV_{CZTS} must equal the junction potential $V_{\mathrm{net}} = V_{bi} - V_{\mathrm{app}}$, where V_{bi} is the built-in voltage determined by the separation of ZnS, CZTS Fermi levels and V_{app} is the externally applied voltage. Hence:

$$\frac{N_d e d^2}{2\varepsilon_{\mathrm{ZnS}}} + \frac{N_a e x_p^2}{2\varepsilon_{\mathrm{CZTS}}} + \frac{\sigma e d}{\varepsilon_{\mathrm{ZnS}}} = V_{\mathrm{net}} \quad \ldots (8)$$

Combining Eqs. (5) and (8) gives a quadratic equation for x_p:

$$\left(\frac{N_a e}{2\varepsilon_{\mathrm{CZTS}}}\right) x_p^2 + \left(\frac{N_a e d}{\varepsilon_{\mathrm{ZnS}}}\right) x_p - \left(V_{\mathrm{net}} + \frac{N_d e d^2}{2\varepsilon_{\mathrm{ZnS}}}\right) = 0 \quad \ldots (9)$$

Since for typical device operating conditions V_{net} is positive it is easy to show that Eq. (9) always gives a unique solution for x_p for any ZnS thickness d. However, since σ is positive, from Eq. (5) the maximum value (d_{max}) for d is $(N_a/N_d)x_p$. This is however the size of the space charge width on the ZnS side for the case of 'bulk' semiconductors. Therefore above d_{max} the junction properties revert to that of Figure 2b.

For the fully depleted case x_p is a function of d and therefore ΔV_{CZTS} is modified (Eq. 7). Ideally x_p should become larger so that ΔV_{CZTS} is increased, thus lowering the electron barrier height ϕ_{B}. A larger x_p also means that the photocurrent collected from the quasi-neutral region of the device is greater. Differentiating Eq. (9) with respect to d gives:

$$N_a e\left(\frac{x_p}{\varepsilon_{\mathrm{CZTS}}} + \frac{d}{\varepsilon_{\mathrm{ZnS}}}\right)\frac{\partial x_p}{\partial d} = \frac{e}{\varepsilon_{\mathrm{ZnS}}}\left(N_d d - N_a x_p\right) \quad \ldots (10)$$

From Eq. (5) the right hand side of Eq. (10) is seen to be negative, so that $(\partial x_p/\partial d)<0$, i.e. the electron barrier height decreases as d becomes smaller. The physical origin of this effect can be explained as follows. The total band bending within the device, i.e. the built-in potential, is fixed by the Fermi level separation between ZnS and CZTS before making contact. As the ZnS

layer thickness is decreased it is expected that the band bending within that layer must decrease, and this is confirmed by Equation (6). The CZTS layer must therefore undergo additional band bending, resulting in a smaller barrier height.

Figure 3 plots the barrier height ϕ_B as a function of ZnS layer thickness, with donor concentrations ranging from 10^{14}-10^{17} cm^{-3}. The CZTS acceptor concentration is fixed at 2 $\cdot 10^{16}$ cm^{-3} following reference [17]. ϕ_B increases monotonically with thickness until it reaches a plateau value, corresponding to 'bulk' ZnS that is no longer fully depleted. The plateau value decreases with ZnS donor concentration, especially in the regime where N_d is larger than N_a. The maximum barrier height for $N_d = 10^{17}$ cm^{-3} is only 0.5 eV. Calculations (see below) show that this is not large enough to produce the experimentally observed current blocking behaviour [2]. Nevertheless plateau values (≥1.7 eV) for all other donor concentrations in Figure 3 produce current blocking, so that in all further calculations it is assumed that $N_d \leq 10^{16}$ cm^{-3}. It should also be pointed out that *n*-type doping is hard to achieve in ZnS due to the presence of acceptor point defects in the form of Zn vacancies [18].

3. Device simulation method

Simulations are carried out to determine the current density (*J*)-voltage (*V*) performance of fully depleted ZnS-CZTS devices. The device stack consists of a transparent conducting oxide (i.e. 250 nm thick Al-doped ZnO and 100 nm of high resistive, intrinsic ZnO), ZnS (variable thickness) and CZTS absorber (2 μm thickness). The TCO and CZTS layer thickness are based on reference [17]. Since the ZnS is directly in contact with the high resistive, intrinsic ZnO the transparent conducting oxide plays little or no part in *pn*-junction equilibrium, so that the junction properties and charge distribution are as described in section 2 for the case of fully depleted ZnS. Even in a conventional CZTS device the electrical properties can be successfully modelled [17] by analysing the CdS-CZTS heterojunction independently of the intrinsic ZnO contact layer. Optical properties of ZnO:Al, *i*-ZnO, ZnS and CZTS were obtained from references [19], [20], [21] and [22] respectively. The intensity of AM1.5 Global solar radiation [23] incident on CZTS was calculated taking into account absorption within the TCO and ZnS layers, as well as reflection at the layer boundaries.

The other ZnS, CZTS materials parameters [24-28] are summarised in Table 1. The simulation assumes thermionic emission of conduction electrons over the barrier. Tunneling is less important due to the low doping density and relatively high temperature [29]. Furthermore, since the ZnS is lattice matched to CZTS there is no interface recombination included in the simulation. Band gap fluctuations [30-33] of 116 meV standard deviation [17] within CZTS are also assumed. Details of the model, which is based on the theory outlined in reference [34], can be found in Appendix A. For simplicity microstructural features, such as grain boundaries and secondary phases in the CZTS absorber layer, are not taken into account. The simulations also assume zero series and infinite shunt resistances. The results reported here should therefore be viewed as the ideal performance values that can be obtained from devices in the fully depleted configuration.

4. Results and Discussion

Figure 4a shows theoretical current density (J)-voltage (V) curves for 50 nm thick ZnS devices. Results are presented for ZnS doping concentrations (N_d) between 10^{14}-10^{16} cm^{-3}. Device properties are summarised in Table 2. With a short circuit current density of ~24 mA/cm^2 (Figure 4a) it is clear that current blocking has been suppressed. Furthermore, since there is no recombination at the lattice matched ZnS-CZTS interface, the V_{oc} is slightly larger than 1.0 V. This is a substantial improvement over the ~0.5 V open circuit voltage values for high performance CZTS devices [6]. The overall efficiencies, i.e. 13.0% for $N_d = 10^{14}$ cm^{-3} and 16.1% for $N_d = 10^{16}$ cm^{-3}, highlight the potential of fully depleted emitter layers, though it should be noted that the calculation does not take into account grain boundaries and any parasitic resistances in the cell. The 'roll over' effect observed close to V_{oc} is due to thermionic emission being suppressed at forward bias (specifically the F_{th} term in Equation A16 rises rapidly above the roll over bias, thereby decreasing the photocurrent; see Appendix A). Figure 4b shows equivalent JV-curves for a 100 nm thick ZnS layer and Table 3 summarises the device properties. The larger barrier height (Figure 3) means that the 'roll over' is more pronounced, resulting in a lower fill factor and hence overall device efficiency (< 8%).

There are several reports [9-11] that provide experimental evidence for current unblocking in ZnS when used as an emitter layer for CZTS(Se) with thickness in the range of 30-60 nm (note however that current unblocking was not observed in reference [35]). In one report [11] the short circuit current density was greater than 25 mA/cm^2. However, the V_{oc} of these ZnS devices was found to be less than the standard CdS emitter layer cells fabricated in the same lab. The expected benefits of lattice matching the ZnS emitter to CZTS absorber layer are therefore not observed. The simulation results shown in Figure 4 did not take into account parasitic resistances in the cell, which for ultra-thin emitter layers can have an important role on device properties, particularly the V_{oc} and fill factor. First pin holes, due to incomplete coverage of ZnS, are likely to be present, so that the shunt resistance is reduced. A high resistive transparent conducting oxide (TCO) layer is required to mitigate the effect of any pin holes. Secondly the relatively small ZnS doping concentration of 10^{14}-10^{16} cm^{-3} would lead to a large series resistance for thin layers. A potential solution is to have ZnS as a thin buffer layer, sandwiched between CdS and CZTS (Figure 2d). Since CdS is highly doped (~10^{18} cm^{-3}; [28]) its space charge region is narrow and forms a highly localised layer of positive charge close to the CdS-ZnS heterointerface. This is similar to the configuration in Figure 2c and it therefore follows that the same arguments for barrier height lowering should be applicable in this case as well. A full analysis of a CdS-ZnS-CZTS junction confirms this to be the case for fully depleted ZnS (see Appendix B; note that interfacial recombination due to lattice misfit between CdS and ZnS is expected to be small due to n-type doping in both layers).

The smaller barrier height for fully depleted emitters means that lattice matching to the absorber layer is the primary criterion for selecting potential emitter/buffer layer materials.

Table 4 lists candidate materials, other than ZnS, that have a small lattice mismatch with CZTS and large band gap ([36]; the latter is desirable for reducing light absorption within the emitter/buffer layer). These compounds have large differences in electron affinity with respect to CZTS, and are therefore current blocking in bulk form. GaP and AlP are the main contenders, due to the extremely small lattice mismatch (<1%). A further advantage is that the fully depleted layers need not be heavily doped when used in the buffer configuration. Indeed N_d = 10^{14} cm^{-3} is sufficient for current unblocking in 50 nm thick ZnS (Figure 4a).

5. Summary

It is shown that the electron barrier due to any intrinsic CB offset can be reduced by making the emitter layer thin enough so that it is fully depleted of carriers. This allows thermionic emission of the photocurrent across the heterojunction. If the emitter material is also lattice matched to the absorber layer then recombination at the heterojunction is minimised, thereby increasing the open circuit voltage. The concept is applied to ZnS-CZTS, where calculated efficiencies as high as 16.1% demonstrate the potential of the method. A possible flaw with the method however is the increased series resistance of the thin emitter layer, which would lower the fill factor and open circuit voltage. This can be mitigated by sandwiching the fully depleted emitter layer between the absorber and another highly doped emitter layer, such as CdS. This bi-layer emitter device retains the benefits of a lower barrier height while also minimising the deleterious effects of parasitic resistances. Finally the less stringent materials demands, i.e. lattice matching only, for a fully depleted emitter configuration means that the materials selection space is larger. For example, GaP and AlP are identified as potential emitter layers for CZTS. These materials are not suitable in bulk form due to a large electron barrier height; their use is only made possible by making the layers thin enough to be fully depleted.

6. Acknowledgements

This work is supported by the Centre for Advanced Materials for Renewable Energy Generation (CAMREG), a consortium led by the University of Edinburgh and funded by the UK Engineering and Physical Sciences Research Council (EPSRC) under grant EP/P007805/1.

References

[1] T.A. Gessert, S.-H. Wei, J. Ma, D.S. Albin, R.G. Dhere, J.N. Duenow, D. Kuciauskas, A. Kanevce, T.M. Barnes, J.M. Burst, W.L. Rance, M.O. Reese, H.R. Moutinho, Research strategies toward improving thin-film CdTe photovoltaic devices beyond 20% conversion efficiency, *Sol. Energy Mat. Sol. Cells* (2013) **119**, 149.

[2] J.T. Wätjen, J. Engman, M. Edoff, C Platzer-Björkman, Direct evidence of current blocking by ZnSe in $Cu_2ZnSnSe_4$ solar cells, *Appl. Phys. Lett.* (2012) **100**, 173510.

[3] A. Nagoya, R. Asahi, G. Kresse, First principles study of Cu_2ZnSnS_4 and the related band offsets for photovoltaic applications, *J. Phys.: Condens. Matter* (2011) **23** 404203.

[4] K. Ito (Editor), *Copper Zinc Tin Sulfide-Based Thin Film Solar Cells*, Wiley (2015).

[5] M.A. Green, Y. Hishikawa, W. Warta, E.D. Dunlop, D.H. Levi, J. Hohl-Ebinger, A.W.H. Ho-Baillie, Solar cell efficiency tables (version 51), *Prog. Photovolt: Res. Appl.* (2018) **26**, 3.

[6] O. Gunawan, T.K. Todorov, D.B. Mitzi, Loss mechanisms in hydrazine-processed $Cu_2ZnSn(Se,S)_4$ solar cells, *Appl. Phys. Lett.* (2010) **97**, 233506.

[7] S. Siebentritt, Why are kesterite solar cells not 20% efficient? *Thin Solid Films* (2013) **535**, 1.

[8] R. Scheer, Activation energy of heterojunction diode currents in the limit of interface recombination, *J. Appl. Phys.* (2009) **105**, 104505.

[9] J. Kim, C. Park, S.M. Pawar, A.I. Inamdar, Y. Jo, J. Han, J. Hong, Y.S. Park, D.-Y. Kim, W. Jung, H. Kim, H. Im, Optimization of sputtered ZnS buffer for Cu_2ZnSnS_4 thin film solar cells, *Thin Solid Films* (2014) **566**, 88.

[10] M. Nguyen, K. Ernits, K.F. Tai, C.F. Ng, S.S. Pramana, W.A. Sasangka, S.K. Batabyal, T. Holopainen, D. Meissner, A. Neisser, L.H. Wong, ZnS buffer layer for $Cu_2ZnSn(SSe)_4$ monograin layer solar cell, *Solar Energy* (2015) **111**, 344.

[11] J.Y. Park, R.B.V. Chalapathy, A.C. Lokhande, C.W. Hong, J.H. Kim, Fabrication of earth abundant $Cu_2ZnSnSSe_4$ (CZTSSe) thin film solar cells with cadmium free zinc sulphide (ZnS) buffer layers, *J. Alloys Cmpds* (2017) **695**, 2652.

[12] J. Bosco, F. Tajdar, H. Atwater, Molecular beam epitaxy of n-type ZnS: a wide band gap emitter for heterojunction PV devices, Proceedings of the 38th IEEE Photovoltaics Specialist Conference, Austin, Texas (2012) p 2513.

[13] W.-C. Hsu, I. Repins, C. Beall, C. DeHart, G. Teeter, B. To, Y. Yang, R. Noufi, The effect of Zn excess on kesterite solar cells, *Sol. Energy Mat. Sol. Cells* (2013) **113**, 160.

[14] J. T. Wätjen, J.J. Scragg, T. Ericson, M. Edoff, C. Platzer-Björkman, Secondary compound formation revealed by transmission electron microscopy at the Cu_2ZnSnS_4/Mo interface, *Thin Solid Films* (2013) **535**, 31.

[15] J. Nelson, *The Physics of Solar Cells*, Imperial College Press, London (2004).

[16] B.G. Mendis, M.C.J. Goodman, J.D. Major, A.A. Taylor, K. Durose, D.P. Halliday, The role of secondary phase precipitation on grain boundary electrical activity in Cu_2ZnSnS_4 (CZTS) photovoltaic absorber layer material, *J. Appl. Phys.* (2012) **112**, 124508.

[17] C. Frisk, T. Ericson, S.-Y. Li, P. Szaniawski, J. Olsson, C. Platzer-Björkman, Combining strong interface recombination with bandgap narrowing and short diffusion length in Cu_2ZnSnS_4 device modelling, *Sol. Energy Mat. Sol. Cells* (2016) **144**, 364.

[18] Y. Gai, J. Li, B. Yao, J.-B. Xia, The bipolar doping of ZnS via native defects and external dopants, *J. Appl. Phys.* (2009) **105**, 113704.

[19] N. Ehrmann, R. Reineke-Koch, Ellipsometric studies on ZnO:Al thin films: refinement of dispersion theories, *Thin Solid Films* **519** (2010) 1475.

[20] H. Yoshikawa, S. Adachi, Opitcal constants of ZnO, *Jpn. J. Appl. Phys.* **36** (1997) 6237.

[21] S. Ozaki, S. Adachi, Optical constants of cubic ZnS, *Jpn. J. Appl. Phys.* **32** (1993) 5008.

[22] S. Adachi, in *Copper Zinc Tin Sulfide-Based Thin Film Solar Cells*, K. Ito editor, Wiley (2015) p. 171.

[23] Air Mass 1.5 Global spectrum obtained from http://rredc.nrel.gov/solar/spectra/am1.5 (NREL Renewable Resource Data Centre).

[24] G.A. Samara, Temperature and pressure dependences of the dielectric constants of semiconductors, *Phys. Rev. B* **27** (1983) 3494.

[25] C.S. Wang, B.M. Klein, First-principles electronic structure of Si Ge, GaP, GaAs, ZnS and ZnSe. I. Self-consistent energy bands, charge densities and effective masses, *Phys. Rev. B* **24** (1981) 3393.

[26] X. Yang, C. Xu, N.C. Giles, Intrinsic electron mobilities in CdSe, CdS, ZnO and ZnS and their use in analysis of temperature-dependent Hall measurements, *J. Appl. Phys.* **104** (2008) 073727.

[27] I.L. Repins, H. Moutinho, S.G. Choi, A. Kanevce, D. Kuciauskas, P. Dippo, C.L. Beall, J. Carapella, C. DeHart, B. Huang, S.H. Wei, Indications of short minority carrier lifetime in kesterite solar cells, *J. Appl. Phys.* **114** (2013) 084507.

[28] M. Gloeckler, A.L. Fahrenbruch, J.R. Sites, Numerical modelling of CIGS and CdTe solar cells: setting the baseline, Proceedings of the 3rd World Conference on Photovoltaic Energy Conversion, Osaka, Japan, 1 (2003) pp. 491-494.

[29] S.M. Sze, *Physics of Semiconductor Devices*, 2nd edition, John Wiley and Sons, New York (1981).

[30] J.J.S. Scragg, L. Choubrac, A. Lafond, T. Ericson, C. Platzer-Björkman, A low temperature order-disorder transition in Cu_2ZnSnS_4 thin films, *Appl. Phys. Lett.* (2014) **104**, 041911.

[31] B.G. Mendis, M.D. Shannon, M.C.J. Goodman, J.D. Major, R. Claridge, D.P. Halliday, K. Durose, Direct observation of Cu, Zn cation disorder in Cu_2ZnSnS_4 solar cell absorber material using aberration corrected scanning transmission electron microscopy, *Prog. Photovolt: Res. Appl.* (2014) **22**, 24.

[32] T. Gokmen, O. Gunawan, T.K. Todorov, D.B. Mitzi, Band tailing and efficiency limitation in kesterite solar cells, *Appl. Phys. Lett.* (2013) **103**, 103506.

[33] B.G. Mendis, A.A. Taylor, M. Guennou, D.M. Berg, M. Arasimowicz, S. Ahmed, H. Deligianni, P.J. Dale, Nanometre-scale optical property fluctuations in Cu_2ZnSnS_4 revealed by low temperature cathodoluminescence, *Sol. Energy Mat. Sol. Cells* (2018) **174**, 65.

[34] S.J. Fonash, *Solar Cell Device Physics*, Academic Press, New York (1981).

[35] D.A.R. Barkhouse, R. Haight, N. Sakai, H. Hiroi, H. Sugimoto, D.B. Mitzi, Cd-free buffer layer materials on $Cu_2ZnSn(S_xSe_{1-x})_4$: band alignments with ZnO, ZnS and In_2S_3, *Appl. Phys. Lett.* (2012) **100**, 193904.

[36] Y. Hinuma, A. Grüneis, G. Kresse, F. Oba, Band alignment of semiconductors from density functional theory and many-body perturbation theory, *Phys. Rev. B* (2014) **90** 155405.

[37] J.H. Werner, J. Mattheis, U. Rau, Efficiency limitations of polycrystalline thin film solar cells: case of $Cu(In,Ga)Se_2$. *Thin Solid Films* **480-481** (2005) 399.

Tables

Property (symbol and units)	**ZnS**	**CZTS**
Relative permittivity (ε, dimensionless)	8.3 [24]	6.5 [17]
Band gap (E_g, eV)	3.73 [3]	1.49 [3]
Electron effective mass (w.r.t electron rest mass)	0.28 [25]	0.19 [17]
Hole effective mass (w.r.t electron rest mass)	1.76 [25]	0.50 [17]
Net donor concentration (N_d, cm^{-3})	10^{14} to 10^{16}	-
Net acceptor concentration (N_a, cm^{-3})	-	$2x10^{16}$ [17]
Electron mobility (μ_n, cm^2/Vs)	249 [26]	26 [17]
Minority carrier lifetime (τ, ns)	-	2 [27]
Band gap fluctuation (σ_g, meV)	-	116 [17]
Conduction band minimum offset (ΔE_c, eV)	1.3 [3]	
Back surface recombination velocity (S_b, cm/s)	10^7 [28]	

Table 1: Materials properties assumed for device simulations. The references from which the values were obtained are as indicated.

N_d (cm^{-3})	J_{sc} (mA/cm^2)	V_{oc} (mV)	Fill factor (%)	Efficiency (%)
10^{14}	23.4	1005	55.1	13.0
10^{15}	23.5	1005	60.6	14.3
10^{16}	23.6	1005	68.1	16.1

Table 2: Device properties for a ZnS-CZTS device with 50 nm thick ZnS layer.

N_d (cm^{-3})	J_{sc} (mA/cm^2)	V_{oc} (mV)	Fill factor (%)	Efficiency (%)
10^{14}	21.9	1005	15.7	3.4
10^{15}	22.0	1005	21.4	4.7
10^{16}	22.2	1005	34.9	7.7

Table 3: Device properties for a ZnS-CZTS device with 100 nm thick ZnS layer.

Compound	Band gap (eV)	Lattice mismatch	Electron affinity difference (eV)
GaP	2.5	0.4%	1.2
AlP	2.7	0.6%	0.9
AlAs	2.4	4.2%	1.0
ZnSe	2.9	4.4%	0.8

Table 4: Potential fully depleted emitter/ buffer layer compounds for CZTS. The band gap, lattice mismatch and electron affinity difference with respect to CZTS is tabulated. Physical properties for the individual compounds were obtained from reference [36].

Figures

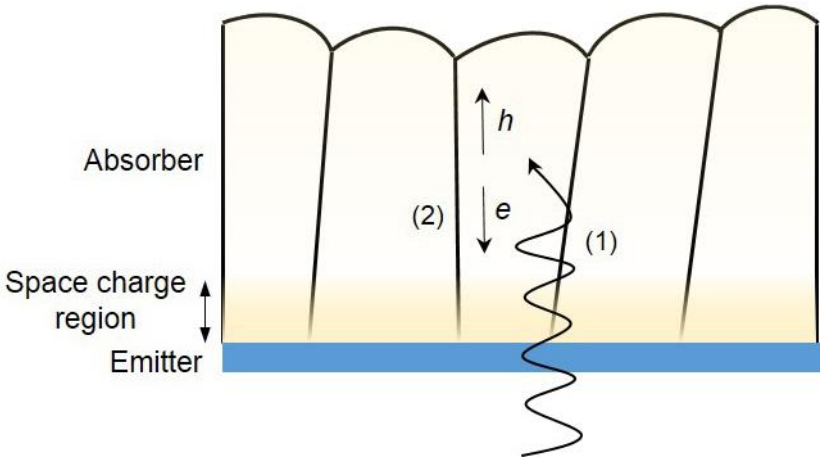

(a)

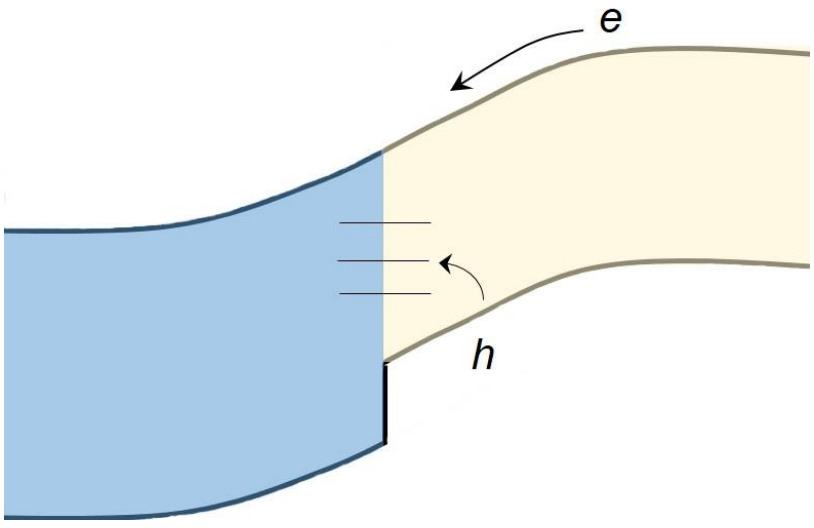

(b)

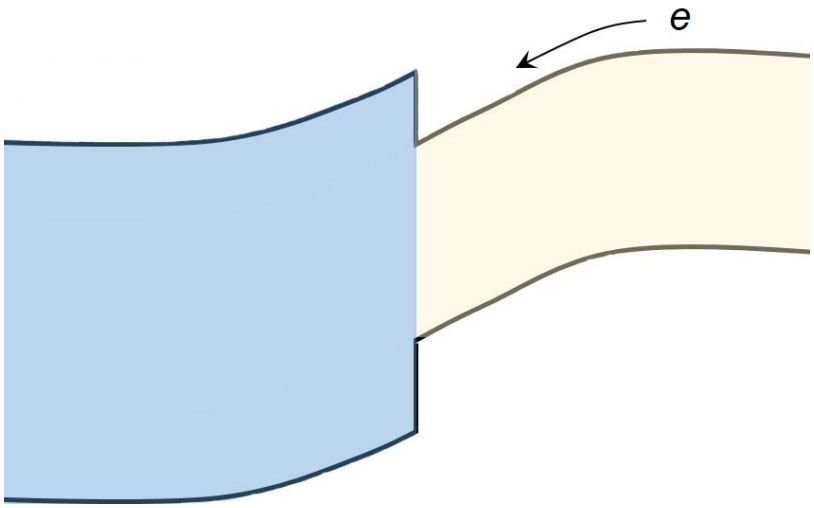

(c)

Figure 1: (a) Schematic illustration of photocurrent generation in a thin-film solar cell. In step (1) the incident light is absorbed within the absorber layer to generate electron (*e*)- hole (*h*) pairs. Photoelectrons that diffuse toward the space charge region in step (2) are collected by the emitter layer. (b) shows the band edge diagram for a lattice mismatched heterojunction with no conduction band (CB) offset. Photoelectrons swept into the space charge region can recombine with holes in the absorber layer via band gap defect states. (c) shows a lattice matched heterojunction with CB offset. Here the electron barrier at the heterointerface gives rise to current blocking.

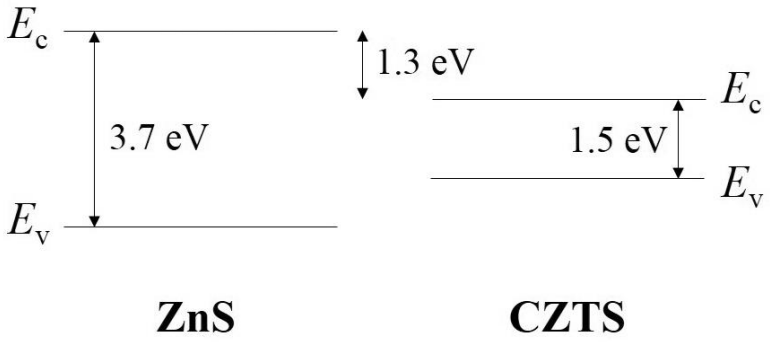

(a)

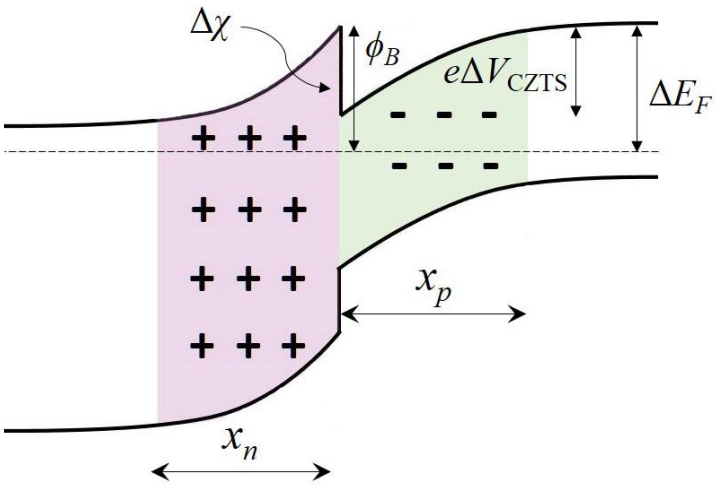
$\Delta\chi$
ϕ_B
$e\Delta V_{CZTS}$
ΔE_F
x_p
x_n

(b)

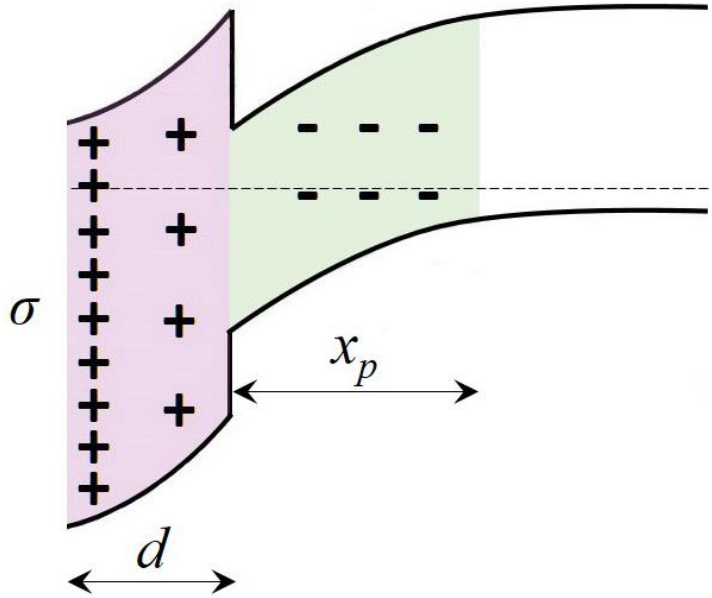
σ
x_p
d

(c)

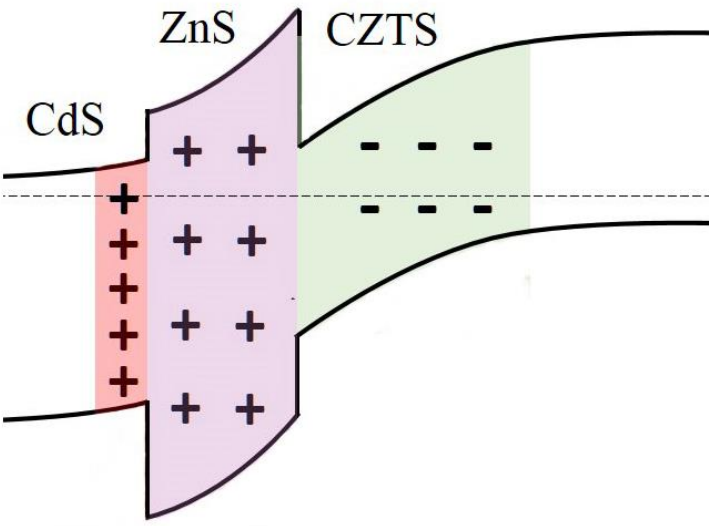
ZnS
CZTS
CdS

(d)

Figure 2: (a) band edge diagram for ZnS and CZTS 'bulk' semiconductors before contact. The conduction band minimum and valence band maximum are denoted by E_c and E_v respectively. (b) shows the equilibrium band edge diagram for the two bulk semiconductors in contact. ZnS and CZTS space charge regions are shaded in purple and green respectively. (c) shows the situation when the ZnS thickness d is sufficiently small for it to be fully depleted. Excess positive charge σ builds up at the ZnS free surface in order to maintain equilibrium. (d) is the band edge diagram for a CdS-ZnS-CZTS system, with the CdS space charge region shaded in red. The horizontal dashed line in Figures 2(b)-2(d) denotes the Fermi level.

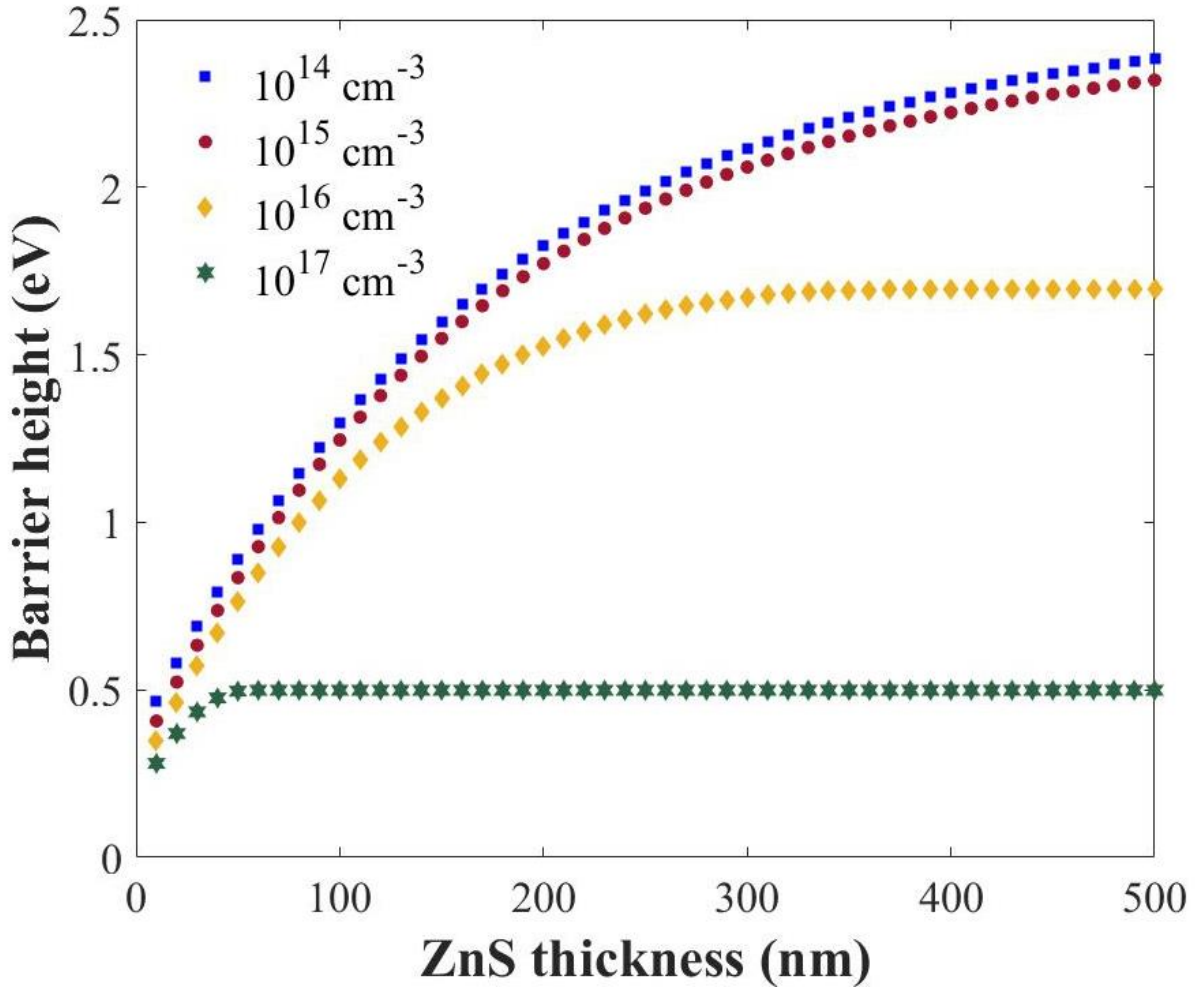

Figure 3: Plot of electron barrier height as a function of ZnS layer thickness for a ZnS-CZTS heterojunction. The CZTS acceptor concentration is fixed at $2 \cdot 10^{16}$ cm^{-3}, while the ZnS donor concentration is varied between 10^{14}-10^{17} cm^{-3}.

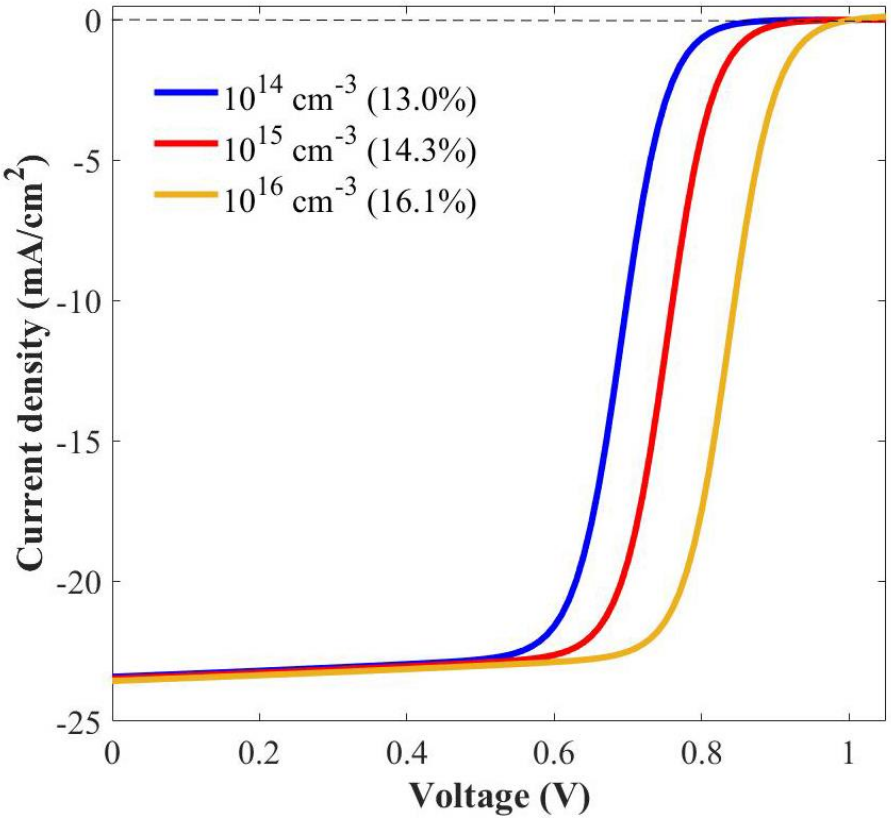
0
-5
-10
-15
-20
-25
0
0.2
0.4
0.6
0.8
1
Current density (mA/cm^2)
Voltage (V)
10^{14} cm^{-3} (13.0%)
10^{15} cm^{-3} (14.3%)
10^{16} cm^{-3} (16.1%)

(a)

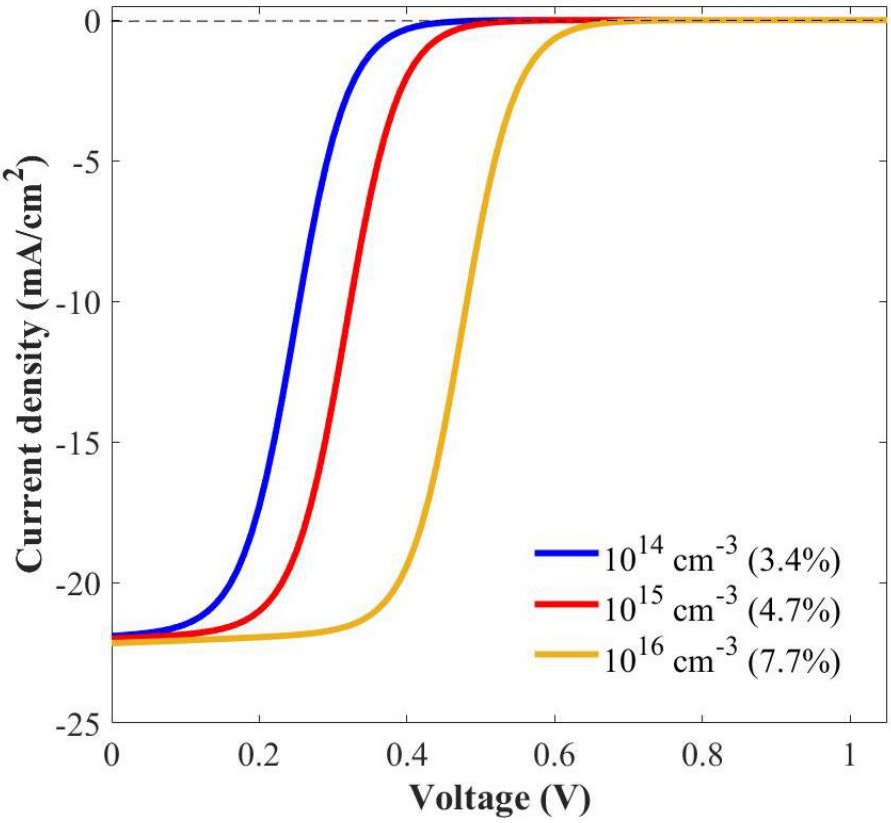
0
-5
-10
-15
-20
-25
0
0.2
0.4
0.6
0.8
1
Current density (mA/cm^2)
Voltage (V)
10^{14} cm^{-3} (3.4%)
10^{15} cm^{-3} (4.7%)
10^{16} cm^{-3} (7.7%)

(b)

Figure 4: Current density-voltage curves for a ZnS-CZTS solar cell under illumination, with (a) 50 nm and (b) 100 nm thick ZnS emitter layer. In each plot the CZTS acceptor concentration is fixed at $2 \cdot 10^{16}$ cm^{-3}, while the ZnS donor concentration is varied between 10^{14}-10^{16} cm^{-3}. The device efficiency is indicated within brackets.

Appendix A: Thermionic emission model for heterojunctions

In this section the thermionic emission model for carrier transport in a fully depleted ZnS-CZTS heterojunction is derived using the theory outlined in reference [34]. The band edge diagram in Figure A1 is used in the calculation, with the ZnS-CZTS interface arbitrarily positioned at $x = 0$. d is the thickness of the ZnS layer, x_p the space charge width on the CZTS side and L the width of the CZTS quasi-neutral region.

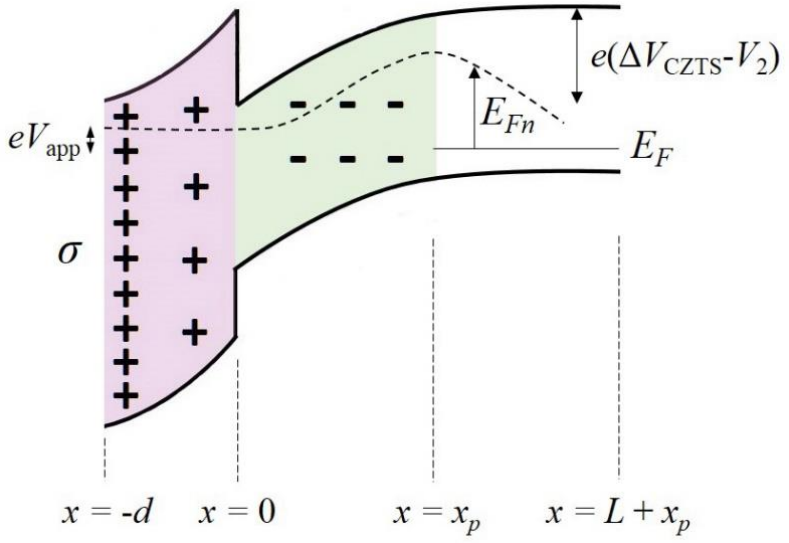

Figure A1: Band edge diagram used for calculating carrier transport in a fully depleted ZnS-CZTS heterojunction. The dashed line is the electron quasi-Fermi level (E_{Fn}) and the line E_F is the equilibrium Fermi level for CZTS.

The electron current in the CZTS quasi-neutral region is due to diffusion and is given by $J_n = eD_n(dn/dx)$, where e is the electron charge, D_n the diffusion coefficient for electrons and 'n' the local electron carrier concentration at position x. The electron carrier concentration within the quasi-neutral region is given by the continuity equation:

$$\frac{d^2n}{dx^2} - \left(\frac{n - n_{p0}}{L_n^{\ 2}} \right) + \frac{\Phi_0}{D_n} \alpha \exp(-\alpha x) = 0 \qquad \ldots (A1)$$

where Φ_0 is the flux incident on the CZTS layer, which has absorption coefficient α, electron diffusion length L_n and an equilibrium electron concentration n_{p0}. Equation (A1) must satisfy the boundary conditions at the back surface and space charge edge respectively, i.e.:

$$D_n\left(\frac{dn}{dx}\right)_{x=L+x_p} = -S_b\left[n(L+x_p) - n_{p0}\right]$$

… (A2)

$$n(x_p) = n_{p0}\exp\left[E_{Fn}(x_p)/kT\right]$$

… (A3)

where S_b is the recombination velocity at the back surface, $E_{Fn}(x_p)$ is the electron quasi-Fermi level at the space charge edge and kT has its usual meaning. E_{Fn} is measured positively upwards with respect to the equilibrium Fermi level in CZTS (see Figure A1). The solution for $J_n(x_p)$ is:

$$J_n(x_p) = J_L - J_{dif}\left\{\exp\left[E_{Fn}(x_p)/kT\right] - 1\right\}$$

… (A4a)

$$J_L = e\Phi_0\left\{\left(\frac{\beta_2{}^2 e^{-\beta_2}e^{-\beta_4}}{\beta_2{}^2 - \beta_1{}^2}\right)\left[\frac{(\beta_3\beta_1/\beta_2) - 1}{\beta_3\sinh\beta_1 + \cosh\beta_1}\right] + \frac{\beta_2{}^2 e^{-\beta_4}}{\beta_2{}^2 - \beta_1{}^2}\left[1 - \left(\frac{\beta_1}{\beta_2}\right)\left(\frac{\beta_3\cosh\beta_1 + \sinh\beta_1}{\beta_3\sinh\beta_1 + \cosh\beta_1}\right)\right]\right\}$$

… (A4b)

$$J_{dif} = \left(\frac{eD_n n_{p0}}{L_n}\right)\left[\frac{\beta_3\cosh\beta_1 + \sinh\beta_1}{\beta_3\sinh\beta_1 + \cosh\beta_1}\right]$$

… (A4c)

where $\beta_1 = (L/L_n)$, $\beta_2 = L\alpha$, $\beta_3 = (L_nS_b/D_n)$ and $\beta_4 = \alpha x_p$. J_L is the photocurrent and J_{dif} is the reverse diode saturation current. n_{p0} in Equation (A4c) can be written as $[(N_cN_v)\exp(-E_g/kT)]/N_a$, where N_c, N_v are the effective density of states of the conduction and valence bands respectively, E_g is the band gap of CZTS with acceptor concentration N_a. Equations (A4a)-(A4c) are for a material with uniform band gap. In CZTS however, band gap fluctuations are present such that:

$$E_g = < E_g > -\sigma_g{}^2/(2kT)$$

… (A5)

where $<E_g>$ is the average band gap and σ_g is the standard deviation in band gap fluctuation. Therefore Equation (A4c) contains an additional multiplicative factor '$\exp[\sigma_g{}^2/(2kT)]$' [37].

The only unknown in Equations (A4a)-(A4c) is $E_{Fn}(x_p)$. The aim is to relate $E_{Fn}(x_p)$ to $E_{Fn}(-d)$, since this is proportional to the applied bias. First $E_{Fn}(x_p)$ is expressed in terms of $E_{Fn}(0^+)$, i.e. the electron quasi-Fermi level at the interface on the CZTS side. The electron concentration within the CZTS space charge region is expressed as:

$$n(x) = n_{p0}e^{\psi_2/kT}e^{E_{Fn}(x)/kT}$$

… (A6)

where ψ_2 is the band bending in the CZTS space charge region, such that positive ψ_2 represents downward bending. ψ_2 for a fully depleted emitter layer heterojunction is calculated using the

method outlined in Section 2. Integrating the expression $J_n = \mu_n n(dE_{Fn}/dx)$ across the space charge region gives:

$$J_{\text{sweep}}^{2n}\int_0^{x_p} e^{-\psi_2/kT}dx\left[e^{E_{Fn}(x_p)/kT} - e^{E_{Fn}(0^+)/kT}\right] = \int_0^{x_p} J_n(x)e^{-\psi_2/kT}dx$$

… (A7a)

$$J_{\text{sweep}}^{2n} = n_{p0}\mu_{n2}kT \Big/ \int_0^{x_p} e^{-\psi_2/kT}dx$$

… (A7b)

Here μ_{n2} is the electron mobility in CZTS. Assuming no recombination within the space charge region, from the continuity equation it follows that $dJ_n/dx = -eG(x)$, where $G(x)$ is the local carrier generation rate. Hence:

$$\begin{aligned} J_n(x) &= J_n(x_p) - e\int_{x_p}^{x} G(x)dx = J_n(x_p) - e\Phi_0\int_{x_p}^{x}\alpha e^{-\alpha x}dx \\ &= J_n(x_p) + e\Phi_0\left[e^{-\alpha x} - e^{-\alpha x_p}\right] \end{aligned}$$

… (A8)

Substituting in Equation (A7a) it follows that:

$$e^{E_{Fn}(x_p)/kT} - 1 = \frac{J_{\text{sweep}}^{2n}}{J_{dif} + J_{\text{sweep}}^{2n}}\left[e^{E_{Fn}(0^+)/kT} - 1\right] + \frac{J_L I_1 + I_2}{\left(J_{dif} + J_{\text{sweep}}^{2n}\right)I_1}$$

... (A9a)

$$I_1 = \int_0^{x_p} e^{-\psi_2/kT}dx \;;\; I_2 = e\Phi_0\int_0^{x_p}\left[e^{-\alpha x} - e^{-\alpha x_p}\right]e^{-\psi_2/kT}dx$$

… (A9b)

So that from Equation (A4a), $J_n(x_p)$ becomes:

$$J_n(x_p) = J_L\left(\frac{J_{\text{sweep}}^{2n}}{J_{dif} + J_{\text{sweep}}^{2n}}\right) - \left(\frac{J_{dif}}{J_{dif} + J_{\text{sweep}}^{2n}}\right)\left(\frac{I_2}{I_1}\right) - \left(\frac{J_{dif}J_{\text{sweep}}^{2n}}{J_{dif} + J_{\text{sweep}}^{2n}}\right)\left[e^{E_{Fn}(0^+)/kT} - 1\right]$$

… (A10)

Next $E_{Fn}(0^+)$ is related to $E_{Fn}(-d)$, which from Figure A1 is equal to eV_{app}, where V_{app} is the applied bias. Thermionic emission takes place from the absorber to emitter layer and vice-versa. The net current flow is [34]:

$$J_{th}\left[e^{E_{Fn}(0^+)/kT}e^{-eV_2/kT} - e^{E_{Fn}(0^-)/kT}e^{-eV_2/kT}\right]$$

… (A11)

here $J_{th} = A^*T^2\exp(-\phi_B/kT)$, where A^* is Richardson's constant and ϕ_B is the electron barrier height. V_2 is the applied bias partitioned on the CZTS side (see Figure A1). Equation (A11) is equal to $[J_n(0) + J_p(0)]$, i.e. the sum of electron and hole currents at the heterojunction. The latter can however be ignored, due to negligible Shockley-Read-Hall recombination at the ZnS-CZTS interface and negligible photocurrent generation within the wide band gap, and thin, ZnS emitter layer. Therefore:

$$J_{th}\left[e^{E_{Fn}(0^+)/kT}e^{-eV_2/kT} - e^{E_{Fn}(0^-)/kT}e^{-eV_2/kT}\right] = J_n(0) \quad \ldots \text{(A12)}$$

The local electron concentration within the ZnS space charge region can be expressed as:

$$n(x) = n_{n0}e^{-eV_{app}/kT}e^{-\psi_1/kT}e^{E_{Fn}(x)/kT} \quad \ldots \text{(A13)}$$

where n_{n0} is the equilibrium electron concentration within the ZnS layer and ψ_1 is the local band bending, such that positive ψ_1 represents upward band bending. Assume negligible generation and recombination of carriers within the wide band gap ZnS layer, so that the electron current within the ZnS space charge region is constant and equal to $J_n(0)$. Integrating $J_n = \mu_n n(dE_{Fn}/dx)$ over the space charge region gives:

$$e^{E_{Fn}(0^-)/kT} - e^{eV_{app}/kT} = J_n(0)/J^{1n}_{sweep} \quad \ldots \text{(A14a)}$$

$$J^{1n}_{sweep} = \mu_{n2}n_{n0}kTe^{-eV_{app}/kT}\Big/\int_{-d}^{0}e^{\psi_1/kT}dx \quad \ldots \text{(A14b)}$$

where μ_{n2} is the electron mobility in ZnS. Substituting Equation (A14a) in (A12) gives:

$$e^{E_{Fn}(0^+)/kT} = e^{eV_{app}/kT} + J_n(0)\left[\frac{1}{J_{th}e^{-eV_2/kT}} + \frac{1}{J^{1n}_{sweep}}\right] \quad \ldots \text{(A15)}$$

Since from Equation (A8), $J_n(0) = J_n(x_p) + e\Phi_0[1-\exp(-\alpha x_p)]$, substituting Equation (A15) in Equation (A10) finally gives:

$$J_n(0) = (F_{2n}/F_{th})J_L - [(1-F_{2n})/F_{th}]\left(\frac{I_2}{I_1}\right) + (e\Phi_0/F_{th})(1-e^{-\alpha x_p}) - (F_{2n}/F_{th})J_{dif}\left[e^{eV_{app}/kT} - 1\right] \quad \ldots \text{(A16a)}$$

$$F_{2n} = J^{2n}_{sweep}/\left(J_{dif} + J^{2n}_{sweep}\right) \quad \ldots \text{(A16b)}$$

$$F_{th} = 1 + \frac{F_{2n} J_{dif}}{J_{th} e^{-eV_2/kT}} + \frac{F_{2n} J_{dif}}{J_{\text{sweep}}^{1n}}$$

… (A16c)

Since $J_p(0) = 0$ the above equation can be used to calculate the total current through the device for any applied bias.

Appendix B: CdS-ZnS-CZTS device equilibrium

In this section junction equilibrium is calculated for a CdS-ZnS-CZTS device. The band edge diagram for such a device is shown in Figure B1. The ZnS layer thickness d is sufficiently small for it to be fully depleted, but the remaining positive charge is now present in the CdS layer, rather than at the free surface. The CdS is highly doped compared to ZnS and CZTS, and therefore the space charge region within the CdS layer is narrow (i.e. $x_n \approx d$, see Figure B1).

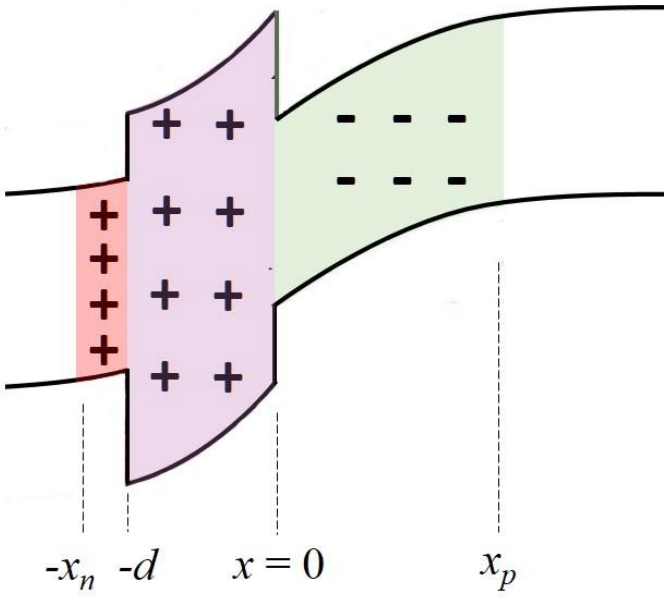

Figure B1: Band edge diagram for a CdS-ZnS-CZTS device, with the ZnS layer fully depleted. The space charge regions for CdS, ZnS and CZTS are represented by red, purple and green shaded areas respectively.

Applying Poisson's equation the electric fields within CdS and ZnS can be shown to be:

$$E_{CdS}(x) = \frac{N_{d(CdS)} e}{\varepsilon_{CdS}} (x + x_n)$$

… (B1)

$$E_{ZnS}(x) = \frac{N_{d(ZnS)} e}{\varepsilon_{ZnS}} (x + d) + \frac{N_{d(CdS)} e}{\varepsilon_{ZnS}} (x_n - d)$$

… (B2)

where $N_{d(CdS)}$, $N_{d(ZnS)}$ are the donor concentrations in the CdS, ZnS layers respectively. The electric fields are chosen such that the boundary conditions are satisfied, i.e. $E_{CdS}(-x_n) = 0$ and $\varepsilon_{CdS}E_{CdS}(-d) = \varepsilon_{ZnS}E_{ZnS}(-d)$. The electric field within CZTS is given by:

$$E_{CZTS}(x) = \frac{N_a e}{\varepsilon_{CZTS}}(x_p - x) \quad \ldots \text{(B3)}$$

Equation (B3) satisfies the boundary condition $E_{CZTS}(x_p) = 0$. The second boundary condition, $\varepsilon_{ZnS}E_{ZnS}(0) = \varepsilon_{CZTS}E_{CZTS}(0)$, leads to the result for charge conservation, i.e.:

$$N_a x_p = N_{d(ZnS)}d + N_{d(CdS)}(x_n - d) \quad \ldots \text{(B4)}$$

The potential change within each of the layers is easily obtained from the electric fields:

$$\Delta V_{CdS} = \frac{N_{d(CdS)}e}{2\varepsilon_{CdS}}(x_n - d)^2 \quad \ldots \text{(B5)}$$

$$\Delta V_{ZnS} = \frac{N_{d(ZnS)}e}{2\varepsilon_{ZnS}}d^2 + \frac{N_{d(CdS)}e}{2\varepsilon_{ZnS}}(x_n - d)d \quad \ldots \text{(B6)}$$

$$\Delta V_{CZTS} = \frac{N_a e}{2\varepsilon_{CZTS}}x_p^2 \quad \ldots \text{(B7)}$$

The sum of Equations (B5) to (B7) must equal the net applied potential V_{net} ($=V_{bi} - V_{app}$), giving the following equation for x_p:

$$\left(\frac{N_a e}{2\varepsilon_{CZTS}} + \frac{N_a^2 e}{2N_{d(CdS)}\varepsilon_{CdS}}\right)x_p^2 + N_a e d\left(\frac{1}{\varepsilon_{ZnS}} - \frac{N_{d(ZnS)}}{N_{d(CdS)}\varepsilon_{CdS}}\right)x_p \ldots - \left[V_{net} + \frac{N_{d(ZnS)}ed^2}{2}\left(\frac{1}{\varepsilon_{ZnS}} - \frac{N_{d(ZnS)}}{N_{d(CdS)}\varepsilon_{CdS}}\right)\right] = 0 \quad \ldots \text{(B8)}$$

Since the CdS doping is large the second term within each round bracket of Equation (B8) is small compared to the first term within the same bracket. The equation for x_p therefore reduces to that derived for a fully depleted ZnS-CZTS heterojunction (cf. Equation (9), main paper). A smaller ZnS layer thickness d therefore increases x_p and consequently the barrier height at the ZnS-CZTS interface is reduced.